Cerebral Cortex, 2023, **33**, 3467–3477
:// . /10.1093/ / 284
Advance access publication date 12 August 2022

P

Yayue Gao[1,†], Guanpeng Chen[2,3,4,†], Pengfei Teng[5], Xin Zhang[6], Fang Fang[2,3,4], Dario J. Englot[7], Guoming Luan[5,8,9,*], Xiongfei Wang[5,8,*], Qian Wang[2,3,10,*]

[1]Department of Psychology, Beihang University, Beijing 100191, China,
[2]

: May 2, 2022. : June 24, 2022. **A** : June 25, 2022

1. Demographic and clinical information of patients with PVNH.

Patient No.	Gender	Age	PVNH	ASO (years)	Epilepsy duration (years)	Seizure frequency (per month)	Interictal epileptiform discharge during MEG recordings (times)
1	M	26	L	23	3	10	< 10
2	M	22	L	20	2	0.25	< 10
3	F	48	L	18	30	3	< 10
4	F	38	L	12	26	1	< 10
5	F	51	L	30	21	1	< 10
6	F	30	L	27	3	0.5	< 10
7	M	19	R	12	7	0.25	10–30
8	M	13	R	7	6	3	0
9	F	13	R	1	12	2	0
10	F	22	R	19	3	1	10–30
11	M	18	R	15	3	3	< 10
12	M	37	R	36	0.9	0.5	0
13	F	23	B	23	0.2	3	30–50
14[a]	F	25	L	19	6	5	/

ASO, age at seizure onset; F, female; M, male; L, left; R, right; B, bilateral. [a]This patient only participated in the sEEG visual experiment.

functionally communicate with neurons in the neocortex over a wide spatial range, which limits our understanding of the potential cognitive relevance of PVNH neurons.

To fill this gap, here we report a quantitative magnetoencephalography (MEG) study of patients with PVNH. We reconstructed spontaneous neural activities in the PVNH tissue and brain-wide areas with high spatial, temporal, and frequency resolution and estimated the inter-areal coupling strength using phase locking values (PLVs; Palva et al. 2018; Arnulfo et al. 2020). We then inspected whether local activities in sensory areas were modulated by their communications with PVNH tissues. In addition, in rare opportunities, we compared visual-evoked responses in the PVNH tissue and the visual cortex in three patients, using MEG-reconstructed signals and sEEG signals, respectively.

Materials and methods

P

From May 2014 to June 2021, 14 patients with PVNH were recruited from the clinical database of epilepsy patients at Sanbo Brain Hospital, Capital Medical University. Thirteen patients participated in the MEG experiment, including six patients with left PVNH tissues, six patients with right PVNH tissues, and one patient with bilateral PVNH tissues (Fig. 1A). None of the patients suffered epileptic seizures during the MEG or sEEG recording. The detailed demographic and clinical information of each patient is shown in Table 1. All patients provided written informed consent in accordance with research protocols approved by the Ethics Committee of the Sanbo Brain Hospital, Capital Medical University.

MEG

Neuromagnetic signals were recorded using a 306-sensor (204 planar gradiometers, 102 magnetometers) whole-head MEG system (Elekta-Neuromag, Helsinki, Finland), sampled at 1,000 Hz. The head position inside MEG was determined by four head position indicator (HPI) coils. The positions of three anatomical landmarks (nasion, left, and right preauricular points), four HPI coils, and at least 150 points on the scalp were digitized before MEG recordings. For each patient, five sequences of 6-min resting-state MEG signals were recorded while the patient was lying (eye closed) in a magnetically shielded recording room. In one patient (P11), two blocks of task-state signals were also recorded.

For MEG source localization purposes, a structural T1-weighted MRI dataset (voxel size: $1 \times 0.5 \times 0.5$ mm^3) was acquired for each patient using a 1.5 T Philips Achieva (Best, The Netherlands) MRI scanner. The cortical reconstruction and segmentation were computed to extract the brain volume, cortex surface, and innermost skull surface based on individual T1-weighted images using the Brainsuite software (http://brainsuite.org/). The whole brain was subsequently parcellated into 130 neocortical areas (65 areas in each hemisphere) according to the USCBrain atlas (Joshi et al. 2020).

The external interference in raw signals was removed by the temporal signal space separation (tSSS) method and then the signals were down-sampled to 400 Hz. Fifty-hertz line-noise and its harmonics were excluded with a band-stop finite impose response filter with a band-stop width of 1 Hz. For each MEG sensor, the continuous signal was then decomposed to spectra-temporal components (Fig. 1B) using Morlet wavelet transforms by *morlet_transform* function in Brainstorm (Tadel et al. 2011) with the cycle number of eight. Twenty-one center frequencies of spectra-temporal components were organized in log space, from 2 to 64 Hz in step of $2^{0.25}$.

F - m

For the continuous signal in each frequency, we performed two types of source estimation. Surface-based and volume-based models were applied to obtain the reconstructed MEG time series in 130 neocortical areas and the PVNH tissue, respectively. All procedures were

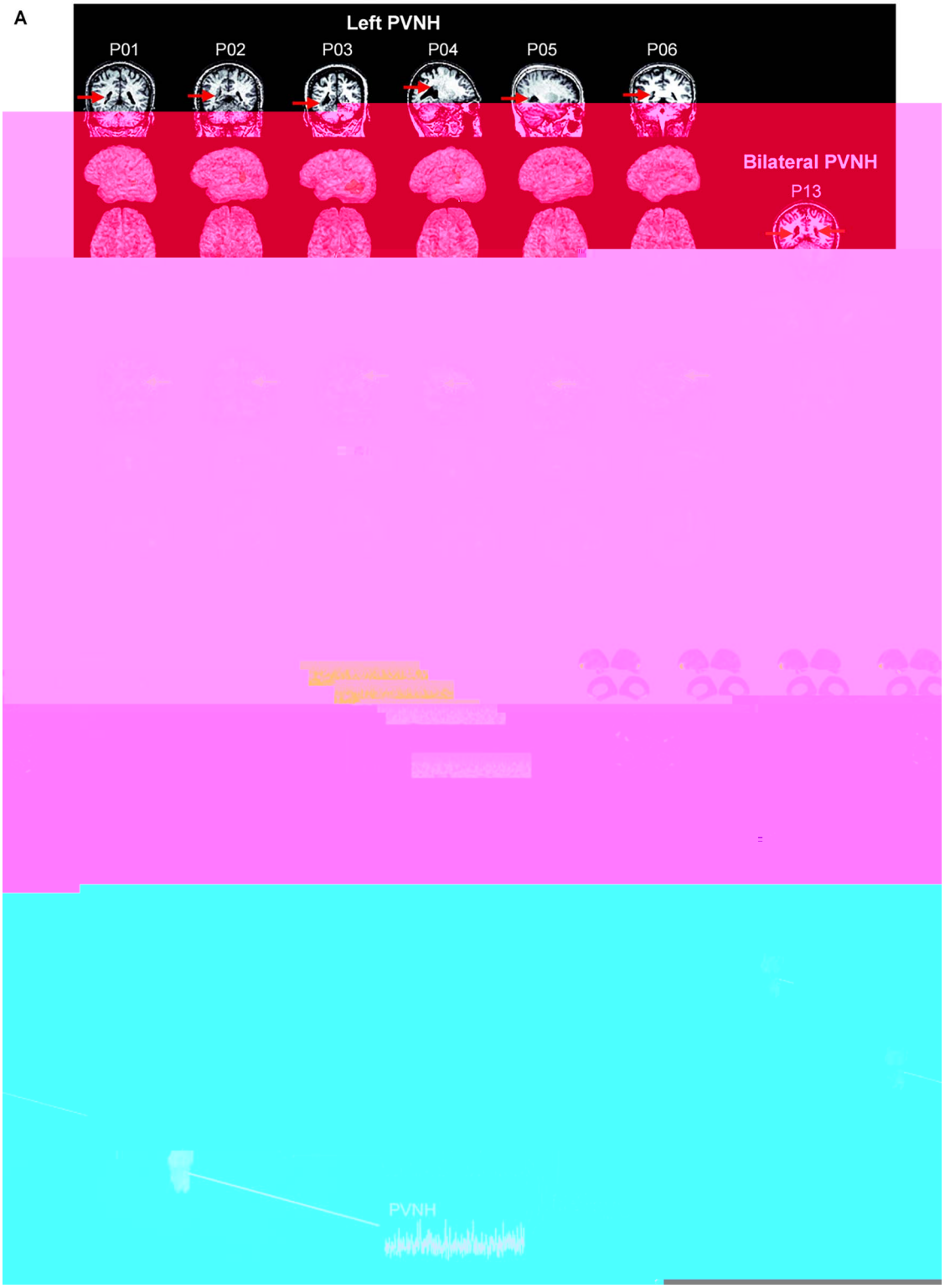

Fig. 1. PVNH localizations and MEG data analysis procedure. **A**) Localizations of PVNH in 13 patients are exhibited in anatomical MR images (T1-weighted) and 3D reconstructed brain models (in lateral and top views), respectively. Red arrows and areas indicate PVNH tissues. **B**) A schematic illustration of the MEG data analysis procedure. The continuous MEG signals were firstly decomposed to spectra-temporal components using Morlet wavelet transforms, logarithmically ranging from 2 to 64 Hz. Then, the source estimation was conducted within each frequency. Inter-areal phase-locking values (PLVs) were calculated between the PVNH tissue and each cortical area in each frequency.

performed on the individual brain model using the Brainstorm toolbox.

For the surface-based source estimation, we computed individual MEG forward models using the overlapping-sphere method with an identity matrix as the noise covariance matrix on the individual pial surface (~15,000 vertices). Then, using the weighted minimum norm estimate (wMNE) model, we obtained source-reconstructed

MEG time series and grouped them into 130 neocortical areas.

For the volume-based source estimation, we also conducted the overlapping-sphere method on the individual

The sEEG recordings were conducted in the ward after electrode implantation, with a sampling rate at 512 Hz (Nicolet Clinical Amplifier, USA). Visual stimuli were displayed on a laptop (refresh rate: 60 Hz; spatial resolution: 1,980 × 1,080; 14-inch, Thinkpad T590). The viewing distance was 42 cm, and the patient's head was stabilized with a chin rest. A full-screen, square-wave grating (radius: 17.8°; spatial frequency: 1 cycle/degree; Michelson contrast: 1; mean luminance: 160.98 cd/m^2) was presented against a gray background (luminance: 22.4 cd/m^2). The orientation of the grating could be one of four possible orientations from 0° to 135° in steps of 45° (relative to the vertical axis). In each trial, the stimulus was presented for 500 ms, followed by a 500-ms blank interval. During the experiment, a total of 80 trials, 20 trials for each orientation, were completed in a random order. The patient was asked to fixate at the fixation point and detect its color change by mouse clicking.

The raw electrophysiological signals were first imported into the EEGLAB toolbox (Delorme and Makeig 2004) and visually inspected for artifact rejections. Then the signals were bandpass filtered at 0.5–200 Hz, epoched starting at 100 ms before stimulus onset and ending at 400 ms after stimulus onset, and corrected for baseline over the 100-ms prestimulus baseline. Visual-evoked potentials were computed by averaging the signals across trials of all four orientations.

[illegible]

In MEG and sEEG visual experiments, we measured the peak latency and the onset latency for each bootstrap sample. First, the peak latency was defined as the time point of the first peak after 50 ms. Second, the onset latency was modified from previously published methods (Raccah et al. 2018; Schrouff et al. 2020) to estimate the time of the inflection point. We divided the response (0–100 ms) into 20-ms bins with 18-ms overlap and extracted the slope by linear fitting. We identified the earliest five consecutive bins with the maximum slope (absolute value) as the response onset.

E[illegible] m[illegible]

In the sEEG visual experiment, P04 and P14 also participated in electrical brain stimulation (EBS) mapping tests for cognitive function evaluation using Nicolet Cortical Stimulator (Natus Neuro, USA). After the recordings of clinical seizures, electrical stimulation was performed through the electrodes in each contact pairs (frequency = 50 Hz, pulse width = 1 ms, duration = 5 s, amplitude from 1.0 to 6.0 mA). Patients were unaware of the timing of the stimulation and the anatomical location of the stimulated structure. During the mapping test, patients were asked to perform a number counting task (speak loudly from 1 to 100). Patients were asked to report immediately if they had any feelings. The results of patients' self-reports were reviewed and further classified by at least one experienced neuropsychologist.

[illegible]

To test the statistical significance of PLVs, we estimated the null distributions of interaction metrics with surrogates that preserved the temporal autocorrelation structure of the original signals while eliminating correlations between two signals. In each iteration, for a signal in the PVNH tissue, we divided the whole time series T into two blocks at a random time point k so that $x\prime_1(t) = x'(1 \ldots k)$ and $x\prime_2(t) = x'(k \ldots T)$, constructed the surrogate as $x\prime_{surr}(t) = [x\prime_2, x\prime_1]$, and computed the surrogate PLVs as in Equation (1). This randomization procedure was repeated 2,000 times. We then averaged surrogate PLVs and obtained a surrogate mean in each patient for further statistical testing.

Permutation tests were applied to estimate the significance of PLV differences by *bst_permtest* in Brainstorm. Pearson correlation was calculated by *corr* function in MATLAB. Bootstrap procedures (5,000 times with replacement) were applied to test the PSD difference against zero and the statistical difference between response latencies. False discovery rate (FDR) corrections were applied to *P*-values involving multiple comparisons, using the *mafdr* function in MATLAB.

Results

P NH [illegible]

At the individual level, we first estimated the spectral property of inter-areal phase synchronization between the PVNH tissue and neocortical areas using source-reconstructed resting-state MEG signals. Generally, as shown in Fig. 2A and Supplementary Fig. 2, both the averaged PVNH-cortical and cortico-cortical PLVs were greater than the surrogate means in a broad frequency scale (from 2.4 to 38 Hz, permutation tests, all $P < 0.005$, FDR corrected). Moreover, to verify the specificity of PVNH-cortical coupling, we also showed that PVNH-cortical PLVs were larger than WM-cortical PLVs in the α–β band (Supplementary Fig. 1, from 4.7 to 27 Hz, permutation tests, all $P < 0.05$, FDR corrected). As shown in whole-brain statistical maps in Fig. 2C and D, after combining PLVs into five frequency bands (δ, 2–4 Hz; θ, 4–8 Hz; α, 8–16 Hz; β, 16–32 Hz; and γ, 32–64 Hz), we identified that both PVNH-cortical and cortico-cortical PLV maps exhibited a peak in the α–β band (permutation tests, all $P < 0.005$, FDR corrected), which was similar to the spectral property of cortico-cortical PLVs in healthy participants (Ghuman et al. 2011).

Next, we asked whether the PVNH-cortical and cortico-cortical PLVs shared a similar spectral property. As shown in Fig. 2A, we found no significant difference between averaged PVNH-cortical and cortico-cortical PLVs in any frequency band (permutation tests, all $P > 0.05$). Furthermore, the correlation coefficients between PVNH-cortical and cortico-cortical PLVs were clustered in the α–β band (Fig. 2B; Pearson correlation, all $P < 0.05$, FDR corrected). In the high-frequency

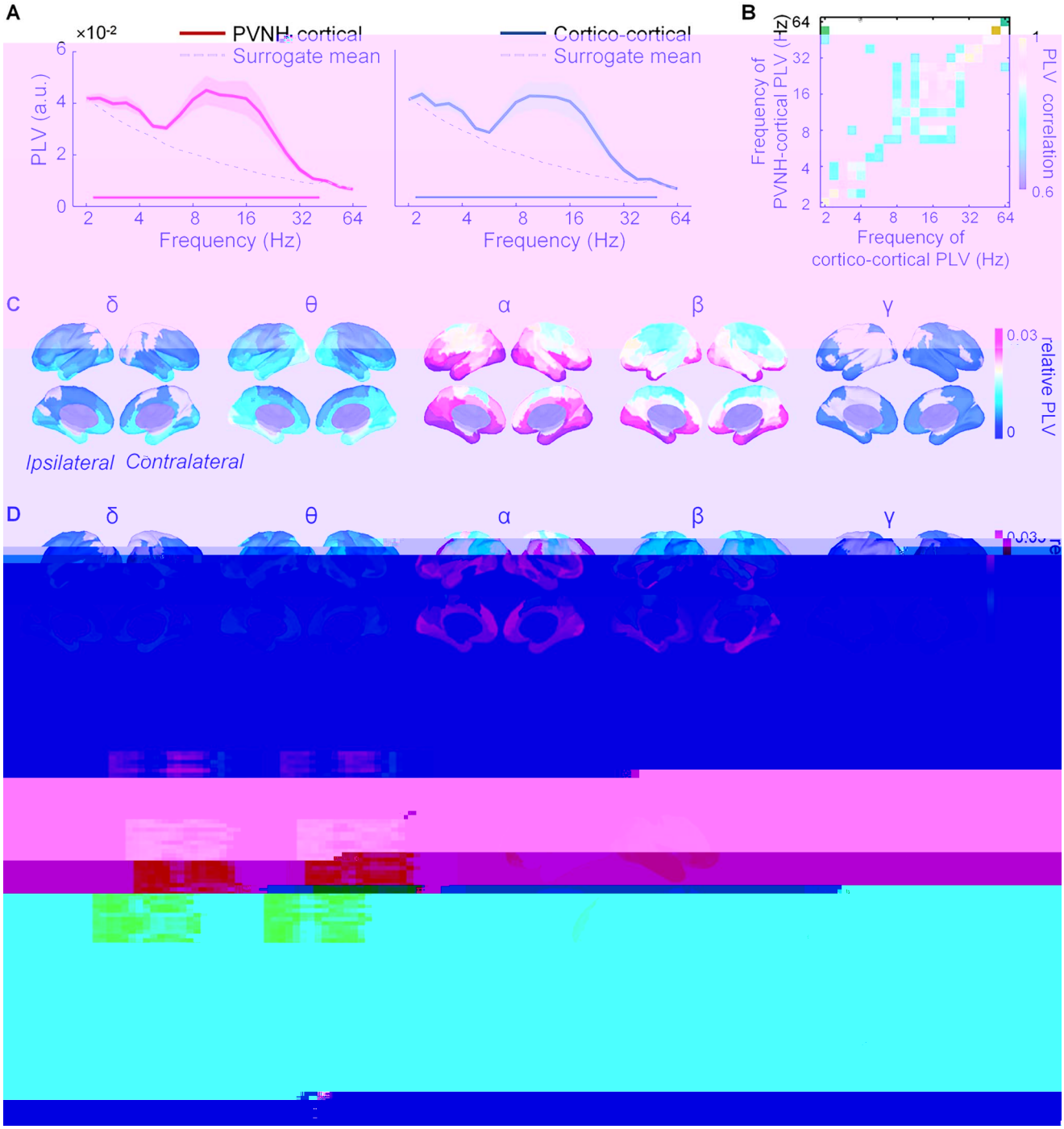

Fig. 2. PVNH-cortical and cortico-cortical PLVs. **A**) Frequency-resolved PVNH-cortical PLVs (*left*) and cortico-cortical PLVs (*right*) are exhibited in colored lines. Shaded areas exhibit SEM of PLVs. Dash lines are the 95th%-ile of the surrogate mean (determined by bootstrap with 5,000 times). Colored bars near the horizontal axis indicate significance (permutation tests, all $P < 0.005$, FDR corrected). **B**) The correlation map between PVNH-cortical PLVs and cortico-cortical PLVs. Only significant correlations were colored (Pearson correlation, all $P < 0.005$, FDR corrected). **C**) Relative PVNH-cortical and **D**) cortico-cortical PLV maps in δ (2–4 Hz), θ (4–8 Hz), α (8–16 Hz), β (16–32 Hz), and γ (32–64 Hz) bands, respectively. The relative PLV equals the absolute PLV minus the surrogate mean in each frequency band. In each cortical area (parcellated using the USCBrain atlas), the averaged PLVs are re-projected to the hemisphere either ipsilateral or contralateral to the individual PVNH location, respectively. Only areas with a PLV greater than the surrogate mean were colored (permutation tests, all $P < 0.005$, FDR corrected). **E**) PVNH-cortical PLVs sorted by the PVNH-cortical distance. Each line represents PLVs in one cortical area. **F**) PVNH-cortical distance maps of the hemispheres ipsilateral and contralateral to the individual PVNH location, respectively. **G**) No correlation between the PVNH-cortical PLV and the PVNH-cortical distance.

band (70–150 Hz), we utilized the envelopes of the high-frequency band amplitudes to obtain the PVNH-cortical and cortico-cortical correlation maps and found they were also similar (Supplementary Methods and Supplementary Fig. 3, Pearson correlation, $r = 0.48$, $P < 0.001$). The similarity between PVNH-cortical and cortico-cortical coupling suggested that PVNH might be involved in the cortico-cortical network.

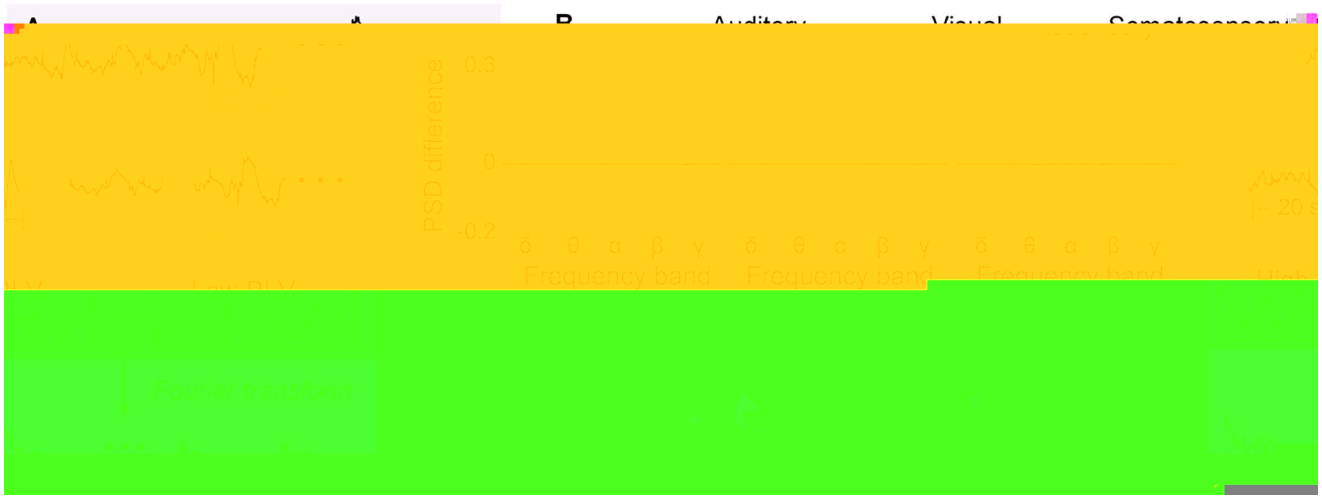

Fig. 3. Local PSDs were associated with the PVNH-cortical PLV fluctuations in sensory areas. **A**) A schematic illustration of PLV-related PSD analysis procedure. Step 1: Source-reconstructed signals were partitioned into 20-s segments; step 2: In each frequency band, segments were sorted by their PLVs, then segments with the highest 10 PLVs (high-PLV group) and the lowest 10 PLVs (low-PLV group) were included in further analyses; step 3: We calculated the PSDs of those two groups of segments using Fourier transform. **B**) Frequency-resolved PSD differences between the high-PLV group and the low-PLV group in bilateral auditory, visual and somatosensory areas. Error bars indicate SEM. *$P < 0.05$, FDR corrected.

Considering the whole brain as a volume conductor, the high PVNH-cortical PLV could be an effect of a short distance between the PVNH tissue and a certain cortical area. To test this possibility, we sorted the frequency-resolved PLVs of cortical areas by their PVNH-cortical distances (Fig. 2E and F). As shown in Fig. 2E, areas near the PVNH tissue did not have stronger PLVs than the other areas in any frequency band. No significant correlation was found between the averaged PVNH-cortical PLV and the PVNH-cortical distance (Fig. 2G; Pearson correlation, $r = -0.016$, $P = 0.853$). These results demonstrated that the PVNH-cortical PLV was not linearly correlated to distance.

P NH- PL

In healthy participants, a major feature of the spontaneous phase coupling in sensory areas was a peak in the α–β band (Ghuman et al. 2011). As shown in Fig. 2C, the PVNH tissue was coupled with sensory areas including auditory, visual, and somatosensory areas in the α–β band, suggesting that the PVNH tissue might be integrated into sensory systems. To further test that, we estimated whether local PSDs in sensory areas were associated with their interactions with PVNH tissues. As shown in Fig. 3A, source-reconstructed signals in bilateral auditory, visual, and somatosensory areas were segmented and sorted by their PVNH-cortical PLVs, respectively. We then calculated the PSDs of time series with the highest PLVs and those with the lowest PLVs and compared the PSD difference with zero. In that case, a significant difference between the PSD difference and zero indicated a co-modulated relationship between the local PSD and the PVNH-cortical PLV in a certain area.

As shown in Fig. 3B, in auditory cortex, higher PVNH-cortical PLVs were associated with lower PSDs in θ band (bootstrap tests, 95% confidence interval [CI] −0.09 to 0.02, $P = 0.02$, FDR corrected). Meanwhile, in visual cortex, the PSDs in the α band were enhanced with higher PVNH-cortical PLVs (bootstrap tests, 95% CI 0.07–0.33, $P = 0.02$, FDR corrected). In somatosensory cortex, no difference between PSDs and zero was found (all $P > 0.05$, FDR corrected). These results suggested that local PSDs in sensory areas were associated with their interactions with PVNH tissues, with distinct spectral characteristics.

P NH

Although our results showed that the PVNH tissue was coupled with sensory areas during the resting state, it remained unknown how the PVNH tissue responded to sensory stimuli and communicated with sensory areas during the task state. To explore that, one patient (P11) also participated in a MEG visual experiment. As shown in Fig. 4A, visual stimuli were presented to P11 during MEG recordings. We reconstructed the visual-evoked activities in both PVNH and the ipsilateral visual cortex. The results showed that both PVNH and visual cortex strongly responded to the visual stimulus presented in the contralateral visual field (Fig. 4B and Supplementary Fig. 4). The remarkable visual-evoked activity in the PVNH tissue might result from projections from either visual cortex or visual thalamus. To verify the hierarchical relationship between the PVNH tissue and visual cortex, we further compared the first peak latencies and the onset latencies (Fig. 4C) of the PVNH tissue and visual cortex at single-trial level, but no significant difference was found (Fig. 4D, bootstrap test, both $P > 0.05$). These results implied a parallel processing of visual information in PVNH and visual cortex neurons.

We further verified this observation via sEEG recordings in a rare opportunity. Another two patients (P04

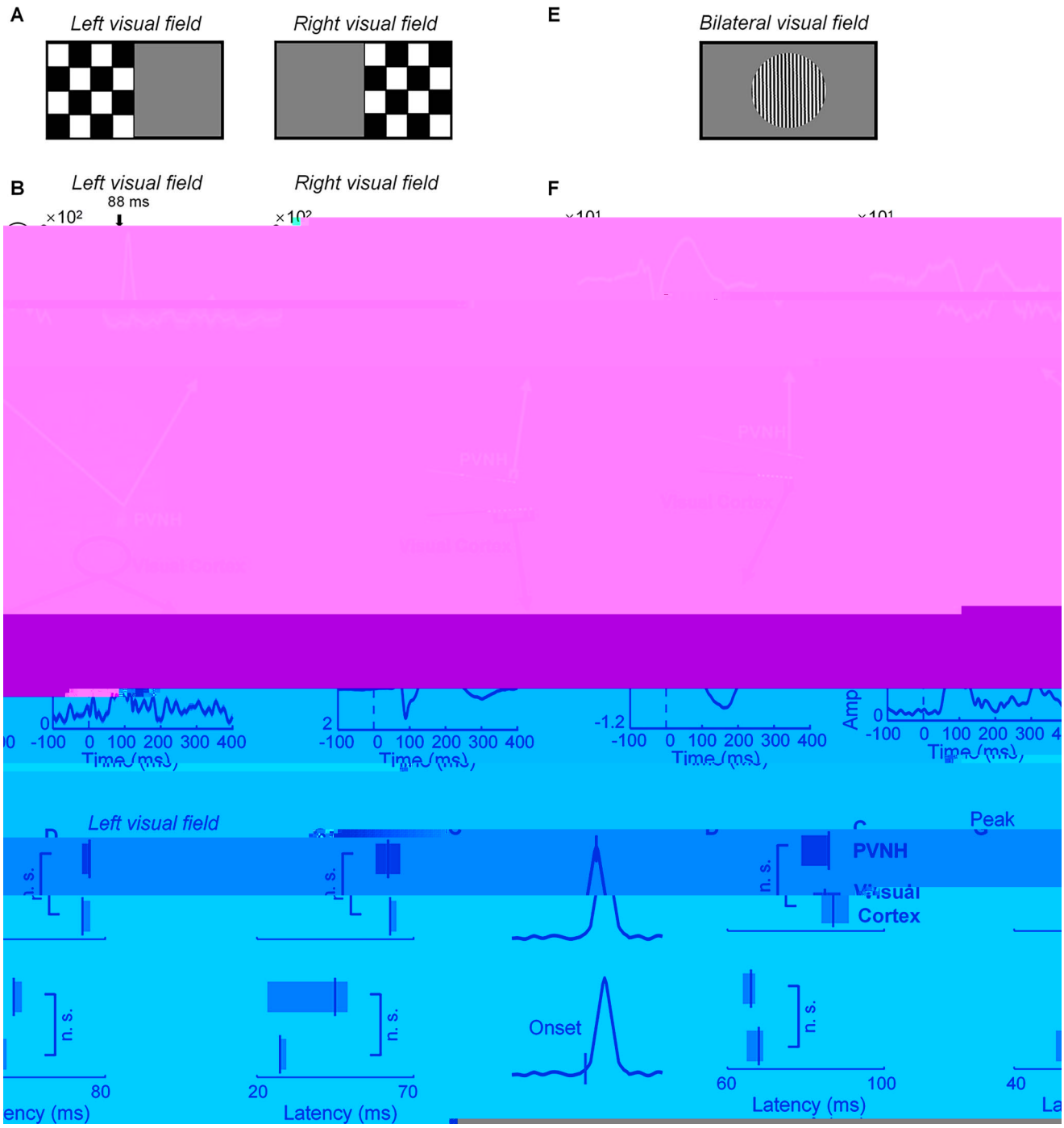

Fig. 4. Visual-evoked activities in PVNH and visual cortex measured by MEG and sEEG. **A**) Visual stimuli used in the MEG visual experiment (P11). **B**) Reconstructed visual-evoked fields estimated by source estimation in the PVNH tissue (*red*) and visual cortex (*blue*), respectively. Shaded areas indicate SEM across trials. Black arrows indicate peak latencies. **C**) A schematic illustration of peak latency and onset latency in responses. **D**) Comparison between latencies of the PVNH tissue (*red*) and those of visual cortex (*blue*) in the MEG visual experiment is shown. **E**) Visual stimuli used in the sEEG visual experiment. **F**) Visual-evoked potentials in P04 (*left*) and P14 (*right*) at contacts within the PVNH tissue (*red*) and visual cortex (*blue*), respectively. **G**) Comparison between latencies of the PVNH tissue (*red*) and those of visual cortex (*blue*) in the sEEG visual experiment is shown. Vertical dashed lines denote the stimulus onset. Shaded areas indicate the 2.5th%-ile–97.5th%-ile confidence interval determined by bootstrap with 5,000 times. *N.s.*: Not significant.

and P14) were implanted with stereo-electrodes in both the PVNH tissue and visual cortex for the preoperative evaluation and participated in the sEEG visual experiment. As shown in Fig. 4F, both contacts located in the PVNH tissue and visual cortex exhibited strong visual-evoked potentials. Similar to the MEG visual experiment, we found no significant difference between the latencies of PVNH and those of visual cortex (Fig. 4G, bootstrap test, all $P > 0.05$). These results further confirmed that the functional activity in PVNH might not result from projections from visual cortex, but rather directly from subcortical structures. The visual

response properties suggested an essential functional role of PVNH.

Besides, P04 and P14 underwent EBS mapping. For the visual responsive contacts we used to calculate visual-evoked potentials, EBS applied to more than half of the visual cortex contacts (4/6) evoked subjective visual percepts (i.e. phosphene) (Supplementary Table 2). However, EBS applied to PVNH contacts ($n = 3$) evoked no visual percepts (Supplementary Table 2). These results implied that the visual responsive PVNH tissue might be functionally homologous with the visual cortical neurons without EBS-evoked percepts.

Discussion

In this study, we applied a state-of-art quantitative analysis approach to characterize the brain-wide inter-areal synchronization in patients with PVNH. Results showed that the synchronization between PVNH and the neocortex and within the neocortex identically predominated in the α–β band during resting and task states. Besides, local neural activities in sensory areas were associated with the coupling strength between these areas and PVNH tissues. Furthermore, in a rare opportunity, we revealed that the PVNH tissue was coactivated with the ipsilateral visual cortex during visual tasks. These results strongly indicate that the PVNH tissue is functionally integrated into neocortical circuits.

Inter-areal coupling at different frequency bands is a general characteristic of the cortical network and is suggested to be an underlying mechanism of neuronal communications in both healthy (Hipp et al. 2012; Bastos et al. 2015; Arnulfo et al. 2020) and epileptic (Englot et al. 2015) brains. Although previous fMRI studies have revealed the functional connectivity between the PVNH tissue and surrounding (Aghakhani et al. 2005; Kobayashi et al. 2006; Tyvaert et al. 2008; Archer et al. 2010; Christodoulou et al. 2012; Liu et al. 2019; Deleo et al. 2020) or distant (Kobayashi et al. 2006; Christodoulou et al. 2012) cortical areas, the oscillatory features of this connectivity are largely unknown. Using whole-brain MEG with high resolution in spectral, temporal, and spatial domains, this study has found two prominent characteristics of the PVNH-cortical coupling in the resting state, which indicate that the PVNH tissue is functionally integrated into neocortical circuits. One is that PVNH-cortical and cortico-cortical PLVs share a similar spectral feature, a peak in the α–β band, which is similar to the spectral property of cortico-cortical PLVs in healthy participants (Ghuman et al. 2011). The other feature is the associated changes between the PVNH-cortical coupling and local neural activities in sensory areas, which has been found in normal cortico-cortical interactions (de Pasquale et al. 2012; Tang et al. 2017). In addition, the PVNH-cortical coupling strength is not linearly correlated to distance. Therefore, our results reveal that PVNH tissue may be coupled with both anatomically near and distant areas of the neocortex via a shared frequency band.

PVNH has long been considered to be related to the pathological brain network which leads to seizures. Previous studies verified the involvement of the PVNH tissue in epileptic networks with the coactivation of the PVNH tissue and seizure onset zones (Valton et al. 2008; Pizzo et al. 2017). However, a recent perspective suggested that there may exist two PVNH-cortical networks, where epileptic tissues in PVNH are connected to epileptic cortical areas (Aghakhani et al. 2005; Tassi et al. 2005), whereas nonepileptic tissues in PVNH are connected to cognitive cortical networks (Akkol et al. 2021). Using sEEG recordings, it was shown that only a portion of recording sites within PVNH tissues generated normal physiological responses and connected to the neocortex (i.e. nonepileptic tissues) during a cognitive task (Akkol et al. 2021). Their findings were partly supported by our current study, which showed that the PVNH tissue could exhibit visual-evoked activities similar to the ipsilateral visual cortex, although we were not able to distinguish neural activities in nonepileptic tissues from those in epileptic tissues in PVNH.

It is not surprising that the PVNH tissue exhibits visual-evoked response which mimics the response in visual cortex ipsilateral to PVNH, in both MEG and sEEG visual experiments. A previous case study found that direct stimulation of the PVNH tissue led to auditory or visual hallucinations (Wagner et al. 2009), suggesting a functional role of PVNH neurons. This assumption is supported by subsequent fMRI and sEEG studies which reveal that the PVNH tissue is activated during multiple cognitive tasks (Christodoulou et al. 2013; Akkol et al. 2021). In this study, we additionally probed the relationship between the activities in the PVNH tissue and visual cortex by measuring the peak latencies. Interestingly, no significant difference between the two response latencies was found, in neither the MEG nor the sEEG visual experiment. One possible explanation is that both the PVNH tissue and visual cortex have matured visual neuron assembly to receive parallel synaptic projections from subcortical structures. That is, although neurons in the PVNH tissue fail to migrate properly, they still have opportunities to develop, mature, and eventually get involved in functional cortical circuits.

Our study has several limitations. First, due to the limited spatial resolution of MEG source localization, we are not able to dissociate MEG signals of epileptic PVNH tissues from those of nonepileptic PVNH tissues. Second, we did not observe any significant phase coupling at high frequencies, which may be restricted by our MEG sampling rate (Arnulfo et al. 2020). Third, as the opportunity to collect these data is extremely rare, we only inspected the visual function in the PVNH tissue, whereas other cognitive functions may also relate to the PVNH tissue (Akkol et al. 2021). These issues should be investigated with advanced approaches in future studies.

In summary, combining MEG and sEEG recordings, we extend our knowledge that ectopic neurons in the PVNH

tissue may retain cognitive functions and be functionally integrated into neocortical circuits, suggesting a potential role for the abnormally migrating neurons in co-development with normally migrating neurons during brain development.

Acknowledgements

We thank Dr Yifei Zhang for his constructive comments on the manuscript.

Supplementary material

Supplementary material is available at *Cerebral Cortex* online.

Funding

National Science and Technology Innovation 2030 Major Program (2022ZD0204804, 2022ZD0204802); the National Natural Science Foundation of China (32171039, 81790650, 81790654, 31930053); Capital's Funds for Health Improvement and Research (2020–4-8012); Institute of Psychology, CAS (No. GJ202005); Opening Project of Key Laboratory of Brain, Cognition and Education Sciences (South China Normal University), Ministry of Education; Beijing Academy of Artificial Intelligence (BAAI); Zhejiang Provincial Natural Science Foundation of China (LGF19H090020); Beihang Univeristy Sponsored Projects for Core Young Researchers in the Disciplines of Social Sciences and Humanities; and R&D Program of Beijing Municipal Education Commission (KM202210025003).

Conflict of interest statement. The authors declare that they have no conflict of interest.

Data availability

The data that support the findings of this study are available from the corresponding author, upon reasonable request.

References

Aghakhani Y, Kinay D, Gotman J, Soualmi L, Andermann F, Olivier A, Dubeau F. The role of periventricular nodular heterotopia in epileptogenesis. *Brain*. 2005:128(3):641–651.

Akkol S, Kucyi A, Hu W, Zhao B, Zhang C, Sava-Segal C, Liu S, Razavi B, Zhang J, Zhang K, et al. Intracranial electroencephalography reveals selective responses to cognitive stimuli in the periventricular heterotopias. *J Neurosci*. 2021:41(17):3870–3878.

Archer JS, Abbott DF, Masterton RAJ, Palmer SM, Jackson GD. Functional MRI interactions between dysplastic nodules and overlying cortex in periventricular nodular heterotopia. *Epilepsy Behav*. 2010:19(4):631–634.

Arnulfo G, Wang SH, Myrov V, Toselli B, Hirvonen J, Fato MM, Nobili L, Cardinale F, Rubino A, Zhigalov A, et al. Long-range phase synchronization of high-frequency oscillations in human cortex. *Nat Commun*. 2020:11(1):5363.

Ayala R, Shu T, Tsai LH. Trekking across the brain: the journey of neuronal migration. *Cell*. 2007:128(1):29–43.

Barkovich AJ, Millen KJ, Dobyns WB. A developmental and genetic classification for midbrain-hindbrain malformations. *Brain*. 2009:132(12):3199–3230.

Bastos AM, Vezoli J, Fries P. Communication through coherence with inter-areal delays. *Curr Opin Neurobiol*. 2015:31:173–180.

Battaglia G, Chiapparini L, Franceschetti S, Freri E, Tassi L, Bassanini S, Villani F, Spreafico R, D'Incerti L, Granata T. Periventricular nodular heterotopia: classification, epileptic history, and genesis of epileptic discharges. *Epilepsia*. 2006:47(1):86–97.

Christodoulou JA, Walker LM, del Tufo SN, Katzir T, Gabrieli JD, Whitfield-Gabrieli S, Chang BS. Abnormal structural and functional brain connectivity in gray matter heterotopia. *Epilepsia*. 2012:53(6):1024–1032.

Christodoulou JA, Barnard ME, del Tufo SN, Katzir T, Whitfield-Gabrieli S, Gabrieli JD, Chang BS. Integration of gray matter nodules into functional cortical circuits in periventricular heterotopia. *Epilepsy Behav*. 2013:29(2):400–406.

de Pasquale F, Della Penna S, Snyder AZ, Marzetti L, Pizzella V, Romani GL, Corbetta M. A cortical core for dynamic integration of functional networks in the resting human brain. *Neuron*. 2012:74(4):753–764.

Deleo F, Hong SJ, Fadaie F, Caldairou B, Krystal S, Bernasconi N, Bernasconi A. Whole-brain multimodal MRI phenotyping of periventricular nodular heterotopia. *Neurology*. 2020:95(17):e2418–e2426.

Delorme A, Makeig S. EEGLAB: an open source toolbox for analysis of single-trial EEG dynamics including independent component analysis. *J Neurosci Methods*. 2004:134(1):9–21.

Englot DJ, Hinkley LB, Kort NS, Imber BS, Mizuiri D, Honma SM, Findlay AM, Garrett C, Cheung PL, Mantle M, et al. Global and regional functional connectivity maps of neural oscillations in focal epilepsy. *Brain*. 2015:138(8):2249–2262.

Ferland RJ, Batiz LF, Neal J, Lian G, Bundock E, Lu J, Hsiao YC, Diamond R, Mei D, Banham AH, et al. Disruption of neural progenitors along the ventricular and subventricular zones in periventricular heterotopia. *Hum Mol Genet*. 2009:18(3):497–516.

Geschwind DH, Rakic P. Cortical evolution: judge the brain by its cover. *Neuron*. 2013:80(3):633–647.

Ghuman AS, McDaniel JR, Martin A. A wavelet-based method for measuring the oscillatory dynamics of resting-state functional connectivity in MEG. *Neuroimage*. 2011:56(1):69–77.

Hipp JF, Hawellek DJ, Corbetta M, Siegel M, Engel AK. Large-scale cortical correlation structure of spontaneous oscillatory activity. *Nat Neurosci*. 2012:15(6):884–890.

Hong SJ, Bernhardt BC, Gill RS, Bernasconi N, Bernasconi A. The spectrum of structural and functional network alterations in malformations of cortical development. *Brain*. 2017:140(8):2133–2143.

Jacobs J, Levan P, Chatillon CE, Olivier A, Dubeau F, Gotman J. High frequency oscillations in intracranial EEGs mark epileptogenicity rather than lesion type. *Brain*. 2009:132(4):1022–1037.

Joshi A, Choi S, Chong M, Sonkar G, Gonzalez-Martinez J, Nair D, Wisnowski J, Haldar J, Shattuck D, Damasio H, et al. A hybrid high-resolution anatomical MRI atlas with sub-parcellation of cortical gyri using resting fMRI. 2020: *bioRxiv*.

Kobayashi E, Bagshaw AP, Grova C, Gotman J, Dubeau F. Grey matter heterotopia: what EEG-fMRI can tell us about epileptogenicity of neuronal migration disorders. *Brain*. 2006:129(2):366–374.

Kothare SV, VanLandingham K, Armon C, Luther JS, Friedman A, Radtke RA. Seizure onset from periventricular

nodular heterotopias: depth-electrode study. *Neurology*. 1998: 51(6):1723–1727.

Liu W, Hu X, An D, Zhou D, Gong Q. Resting-state functional connectivity alterations in periventricular nodular heterotopia related epilepsy. *Sci Rep*. 2019:9(1):18473.

Nadarajah B, Parnavelas JG. Modes of neuronal migration in the developing cerebral cortex. *Nat Rev Neurosci*. 2002:3(6):423–432.

Palva JM, Wang SH, Palva S, Zhigalov A, Monto S, Brookes MJ, Schoffelen JM, Jerbi K. Ghost interactions in MEG/EEG source space: a note of caution on inter-areal coupling measures. *Neuroimage*. 2018:173:632–643.

Pizzo F, Roehri N, Catenoix H, Medina S, McGonigal A, Giusiano B, Carron R, Scavarda D, Ostrowsky K, Lepine A, et al. Epileptogenic networks in nodular heterotopia: a stereoelectroencephalography study. *Epilepsia*. 2017:58(12):2112–2123.

Raccah O, Daitch AL, Kucyi A, Parvizi J. Direct cortical recordings suggest temporal order of task-evoked responses in human dorsal attention and default networks. *J Neurosci*. 2018: 38(48):10305–10313.

Rakic P. Neuron-glia relationship during granule cell migration in developing cerebellar cortex. A Golgi and electonmicroscopic study in Macacus rhesus. *J Comp Neurol*. 1971:141(3):283–312.

Rakic P. Specification of cerebral cortical areas. *Science*. 1988: 241(4862):170–176.

Rakic P. Evolution of the neocortex: a perspective from developmental biology. *Nat Rev Neurosci*. 2009:10(10):724–735.

Schrouff J, Raccah O, Baek S, Rangarajan V, Salehi S, Mourao-Miranda J, Helili Z, Daitch AL, Parvizi J. Fast temporal dynamics and causal relevance of face processing in the human temporal cortex. *Nat Commun*. 2020:11(1):656.

Tadel F, Baillet S, Mosher JC, Pantazis D, Leahy RM. Brainstorm: a user-friendly application for MEG/EEG analysis. *Intell Neurosci*. 2011:2011:1–13.

Tang W, Liu H, Douw L, Kramer MA, Eden UT, Hamalainen MS, Stufflebeam SM. Dynamic connectivity modulates local activity in the core regions of the default-mode network. *Proc Natl Acad Sci U S A*. 2017:114(36):9713–9718.

Tassi L, Colombo N, Cossu M, Mai R, Francione S, Lo Russo G, Galli C, Bramerio M, Battaglia G, Garbelli R, et al. Electroclinical, MRI and neuropathological study of 10 patients with nodular heterotopia, with surgical outcomes. *Brain*. 2005:128(Pt 2):321–337.

Tyvaert L, Hawco C, Kobayashi E, LeVan P, Dubeau F, Gotman J. Different structures involved during ictal and interictal epileptic activity in malformations of cortical development: an EEG-fMRI study. *Brain*. 2008:131(8):2042–2060.

Valton L, Guye M, McGonigal A, Marquis P, Wendling F, Régis J, Chauvel P, Bartolomei F. Functional interactions in brain networks underlying epileptic seizures in bilateral diffuse periventricular heterotopia. *Clin Neurophysiol*. 2008:119(1):212–223.

Wagner J, Elger CE, Urbach H, Bien CG. Electric stimulation of periventricular heterotopia: participation in higher cerebral functions. *Epilepsy Behav*. 2009:14(2):425–428.